Total elastic-scattering cross sections for metastable Ar on Kr

H. Li,* E. S. Gillman,† J. W. Sheldon, and K. A. Hardy
Florida International University, Miami, Florida 33199
(Received 17 June 1991; revised manuscript received 21 August 1991)

Velocity-dependent total elastic-scattering cross sections are measured for metastable argon scattered from krypton in the velocity range 500 to 5000 m/sec. An interaction potential for the reaction is derived from the data by both a semiclassical analysis and a full quantum calculation. The results are compared with previous measurements.

PACS number(s): 34.40.+n, 34.20.Cf, 82.20.Kh

I. INTRODUCTION

The metastable argon-krypton (Ar^*+Kr) atom-atom potential has been extensively studied for the past several years by several investigators. Studies of this reaction have used both differential and integral elastic-scattering-cross-section measurements. These measurements have led to no agreement on the value of the parameters to use for the potential to describe this reaction. The long-range term of all the potentials used for this reaction is the induced-dipole–induced-dipole or van der Waals attractive terms, C_6/r^6. The values quoted for this term vary widely, and, in most cases, show little agreement with the C_6 term used to describe the interaction between the electronically similar K in the reaction $K+Kr$. We investigated the Ar^*+Kr reaction in order to better determine the interaction potential between these two gasses. This reaction is of interest in discharge theory and the theory of $Ar+Kr$ lasers.

Total elastic-scattering cross sections are but one method used to deduce the atom-atom interaction potential between two atomic species. Studies of the Ar^*+Kr interaction have been made by both Martin *et al.* [1] and Winicur *et al.* [2], who measured differential cross sections using a supersonic crossed-beam apparatus. Total elastic-scattering cross sections have been measured for the interaction by Nenner [3] using a supersonic argon beam, excited by electrons, seeded with varying amounts of hydrogen, and interacting with krypton in a collision cell. Kerstel *et al.* [4] measured the total elastic-scattering cross section using a crossed-beam apparatus with both supersonic and plasma discharge sources for the metastable argon beam and a supersonic krypton beam as the target.

II. APPARATUS

The apparatus used in these experiments has been described earlier [5-7]. Figure 1 shows the equipment. Briefly, it is comprised of a vacuum envelope consisting of two differentially pumped chambers. The pressure in the chamber containing the source is maintained at about 1.5×10^{-5} Torr and at about 2×10^{-6} Torr in the chamber containing the scattering cell and the detector. The source of the metastable atoms is a gas discharge in a pyrex tube approximately 3.1 cm long. Metastable argon atoms effuse through a 9.5×0.2-mm slit in the end of the discharge tube. The gas supplied to the discharge is research-grade argon and is supplied through an automatic pressure controller to keep the source pressure constant during a particular experimental run. In these experiments the source pressures used were in the range of 35–60 mTorr. Electrons are supplied to the discharge by a thoria-coated tungsten ribbon. The discharge voltage was approximately 50 V, and the discharge current was maintained at about 260 mA. by varying the filament current. No separation of the $^3P_{2,0}$ states was attempted, however, in other works [8] with a similar beam source the $^3P_2$ states were shown to dominate by about 6 to 1 over $^3P_0$.

The beam chopper, located downstream of the discharge, is a rotating disk driven by a synchronous motor. The disk is 5.8 cm in diameter and has two opposed 1.5×0.75-mm slits. The velocity resolution of the apparatus is a function of the velocity and, in these experiments, varied from 1.2% at a velocity of 500 m/sec to 38% at a velocity of 5.5 km/sec. Before entering the main chamber containing the scattering cell and detector system, the beam passes through a 500-V/cm electric field which removes any charge particles and possible Rydberg states.

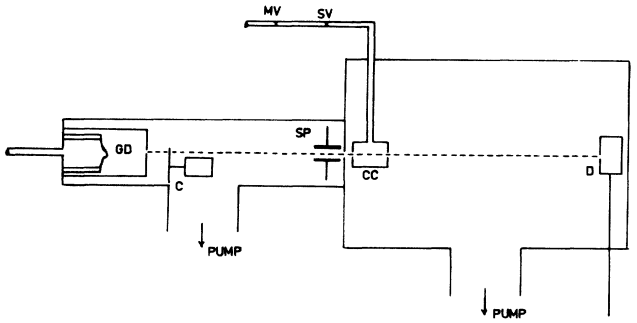

FIG. 1. Scattering apparatus. GD, gas discharge; *C*, beam chopper; SP, sweep plates; (500 V/cm electric field); CC, collision cell; *D*, channeltron detector; MV, metering valve; and SV, computer-controlled solenoid valve. See text for additional details.

The target krypton gas is admitted to the scattering cell by a computer-controlled valve so that the gas can be cycled in and out of the scattering cell during an experimental run. The measurement of pressure in the scattering cell is crucial for obtaining accurate total scattering cross-section measurements, and, in this experiment, the pressure was monitored by two independent systems. A Datametrics Model 1014A electronic capacitance manometer's analogue output was digitized and monitored by the data acquisition computer at the beginning and end of each gas-in and gas-out cycle. This measurement was checked by manually monitoring the pressure recorded by a second electronic capacitance manometer, a MKS model 390. (This second manometer has recently been calibrated by the manufacturer with standards traceable to the National Institute of Standards.) A small correction (1.7%) to the measured pressure was made to compensate for the difference in temperature between the manometers and the collision cell [9].

The detector is located 40 cm from the exit of the collision cell and has an entrance slit 9.5×.28 mm. The beam geometry gives an angular resolution of 1.8′ by the Kusch criterion [10]. Auger electrons produced by Ar* atoms in the detector are guided into a channeltron electron multiplier. The output pulses of the multiplier are counted by the data acquisition computer (Tracor Northern TN-11) and stored for analysis.

III. RESULTS

The data were acquired by measuring the velocity distribution with gas in the collision cell, evacuating the collision cell, and measuring the velocity distribution with gas out of the collision cell. Counting intervals were 5 min for gas in and 5 min for gas out. At the end of each gas-in–gas-out cycle, the beam intensity was monitored, and, if the intensity was within preset limits, the counts acquired were added to counts already accumulated. This procedure would partially compensate for the effects of any long-term drift in the beam intensity. In addition, the pressure in the scattering cell was measured at the beginning and end of each counting cycle.

Figure 2 shows the data from a typical experimental run. The large peak in the data is the typical Maxwellian time-of-flight distribution expected from an effusive source, while the smaller peak is the fast metastable argon peak [11]. The existence of the fast peak gives a useful relative velocity range in this experiment of 325–5000 m/sec. The beam velocities $V_b = L/t$ were obtained from the beam path length L (73 cm) for each flight time. The time-of-flight (TOF) intensity distributions, $I_i(t)$ and $I_0(t)$ with and without Kr in the collision cell, respectively, are shown with background counts subtracted. The effective total cross sections, $Q(V_b)$ were calculated from the expression

$$Q(V_b) = \left[\frac{kT}{PL}\right] \ln \frac{I_0(t)}{I_i(t)} , \tag{1}$$

where k is Boltzmann's constant, P and T are the collision cell pressure and temperature, and L is the collision cell length. A correction to the collision cell length to account for nonuniform target gas density along the beam path through the cell was considered. Since, according to the calculations of Nelson and Colgate [12], such a correction would be less than 0.29%, it has been neglected. $Q(V_b)$ is related to the relative velocity-dependent apparent total scattering cross section $Q_a(g)$

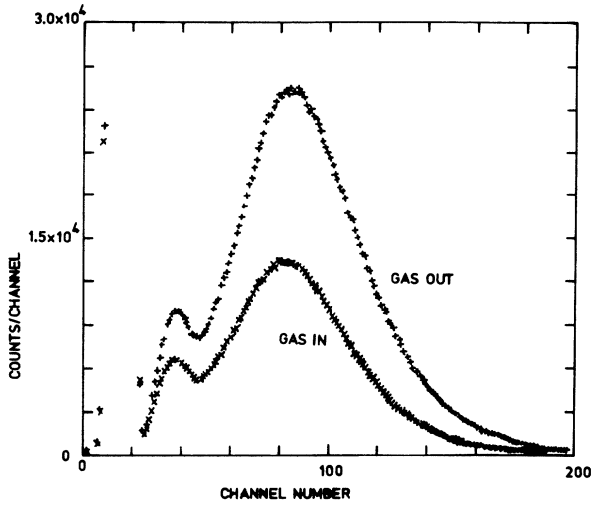

FIG. 2. Metastable argon TOF spectra. The abscissa is the channel number, with the time calibration 1.3 msec/channel. The smaller peak on the left is due to the fast metastable argon, while the large peak is the normal Maxwellian time distribution.

$$Q(v_b) = \int_{\vec{v}} F(\vec{v}_t) \frac{g}{v_b} Q_a(g) d\vec{v}_t , \tag{2}$$

where g is the relative velocity of the collision and $F(\vec{v}_t)d\vec{v}_t$ is the velocity distribution of the target Kr.

The apparent total scattering cross section $Q_s(\bar{g})$, as a function of $\bar{g}$ the relative velocity averaged over the target gas velocity distribution, is obtained from the expression given by Lang *et al.* [13],

$$Q_a(\bar{g}) = \frac{V_b}{\bar{g}} \frac{Q(v_b)}{f(s,x)} , \tag{3}$$

where $x = v_b/v_p$ and v_p is the most probable velocity of the Kr in the collision cell. In deriving Eq. (3) it is assumed that the long-range attractive potential is proportional to $1/r^s$. Tabulated values of the function $f(s,x)$ given by Lang *et al.* [13] are used here, however, they never vary by more than 3% from unity for our experimental conditions. It should also be noted that $f(s,x)$ is almost independent of s ($4 \le s \le 18$).

In order to get the integral elastic-scattering cross section, Q_e from Q_a, two additional effects must be considered, the finite angular resolution of the apparatus and the contribution of inelastic events to the beam attenuation. The inelastic cross section has beam measured by Bourene and Le Calve [14], Piper *et al.* [15], and Winicur *et al.* [12]. The latter give a fit of all these results to the empirical equation, suggested by Eu and Liu [16],

$$Q_i(g) = Q_{i0}[1-(g_0/g)^2]^{1/2} , \tag{4}$$

TABLE I. Semiclassical model parameters in Eq. (8).

	This work		
Parameter	C_2 free	$C_2=0.4$	Ref. [4]
C_1	486.4 (Å^2)	485.5 (Å^2)	621.9 (Å^2)
C_2	0.362	0.4	0.3234
C_3	−31.0 (Å^2)	−36.20 (Å^2)	38.5 (Å^2)
C_4	13.89 (Å^2)	16.71 (Å^2)	0.05 (Å^2)
C_5	0.0237	0.615	2.1252
C_6	10.54	9.24	12.138
C_7	0.0989	0.257	−0.3666
ε		6.74	8.72
r_m		5.02	5.12

where $Q_{i0}=10.62$ Å^2 and $g_0=435$ m/sec.

Due to the finite angular resolution of the apparatus, some atoms, scattered through small angles in the laboratory system, reach the detector and thereby reduce the measured cross section. The correction to the elastic-scattering cross section to account for this small-angle scattering was given by von Busch [17] as

$$\frac{\Delta Q}{Q_e}=0.066\,46 Q_e^{1/2}\gamma k^2(1+0.374x^{-2}) , \tag{5}$$

where $k=m_b V_b/\hbar$ is the beam wave number and $\gamma=F\theta_r$. The F factor is determined by the beam profile and the detector width and is given by von Busch [17] for the present qeometry as 4.0. Using the complete integral cross section, $Q_e=Q_a+\Delta Q$, the correction can be approximated in terms of the measured Q_a by

$$\Delta Q=\frac{0.066\,46 Q_a^{3/2}}{1-(3/2)Q_a^{1/2}}\gamma k^2(1+0.374x^{-2}) . \tag{6}$$

We have used this expression rather than using the usual iterative procedure [3] to make the correction.

The corrected integral elastic-scattering cross section is then obtained from

$$Q_e(\bar{g})=Q(\bar{g})+\Delta Q(\bar{g})-Q_i(\bar{g}) . \tag{7}$$

A total of 18 experimental runs were made with counting times of up to 14 h in an individual experimental run. The cross sections from each experimental run were computed and then the final cross sections were determined by a weighted average of the individual runs. the pressures in the scattering cell were varied from run to run to minimize random error in the pressure determination. The pressures varied from 0.091 to 0.216 mTorr in these experiments.

IV. DISCUSSION

A. Semiclassical analysis

The data have been analyzed by both a semiclassical model following Kerstel *et al.* [4] and a full quantum cal-

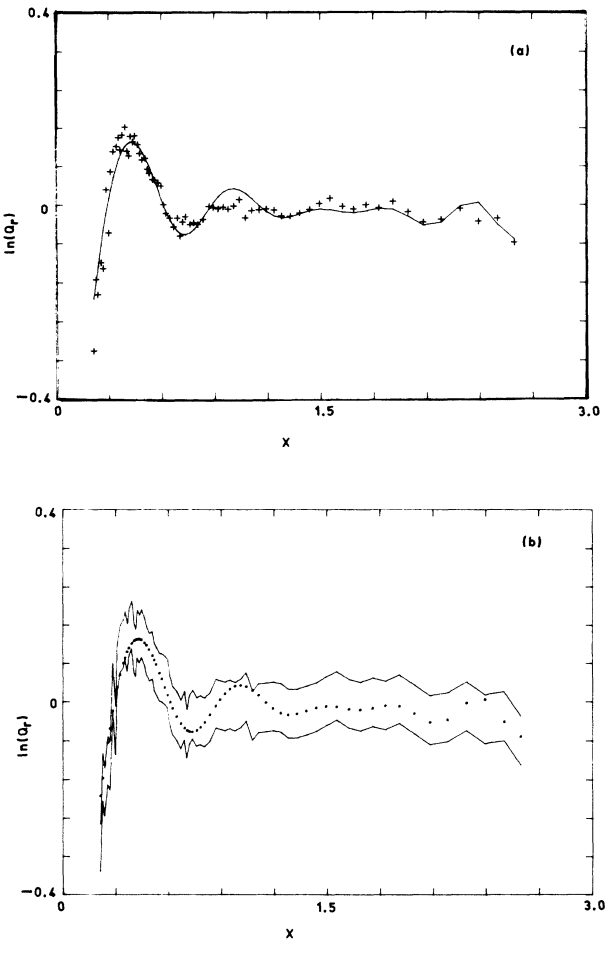

FIG. 3. Reduced cross sections. (a) Comparison of the experimental data (+), with the semiclassical model. A line is drawn through the points at which the semiclassical model function was calculated. (b) The fit to the model function (.). The points are the points at which the model function was calculated. The solid lines indicate the upper and lower extent of the error on the experimental data points.

TABLE II. Model potential parameters. Atomic units are used.

Potential Eq.	Parameters						
	A	*B*	*C*	*D*	*C*6	*C*8	*C*10
(9)							
(10a);(10b)	1.58×10^{7}	11			340	1.00×10^{5}	6
(10a);(10c)	1.58×10^{4}	−53.0	0.264	1.80	281	1.50×10^{4}	1.00×10^{5}
(10a);(10d)	5.27	8.46	13.56	15.41	274	1.238×10^{4}	4.92×10^{4}

[a]Not used.

culation of the phase shifts. The semiclassical model function is given by

$$Q=Q_a+Q_{gl}\ ,$$
$$Q_a=C_1X^{C2}\ ,$$
$$Q_{gl}=A_{gl}\sin(\theta_{gl})\ , \tag{8}$$
$$A_{gl}=C_3X^{-1/2}+C_4X^{3/2}\ ,$$
$$\theta_{gl}=C_5+C_6X+C_7X^3\ ,$$

where the inverse relative velocity $X=1000(\bar{g}^{-1})$. The seven C_i parameters were the free parameters in the model function. The experimental cross sections [the $Q_e(\bar{g})$ from Eq. (7)] were fit by a nonlinear least-squares program, and the parameters giving the best fit are presented in Table I. Q_1 has the form of the Landau-Lifshitz cross section with $C_2=2/(s-1)$, where the long-range potential has an r^{-s} radial dependence. Therefore, the value of $C_2=0.362$ corresponds to a long-range potential, $-C_*r^{-6.52}$. The Landau-Lifshitz cross section for this potential,

$$Q_1=7.7507(C_*/\hbar g)^{0.362}\ ,$$

can be used to obtain $C_*=1430$ a.u.

The value of the constant, C_2, corresponds to a long-range attractive potential of $C^*/r^{6.52}$. This may be interpreted to mean that there are substantial contributions from $1/r^8$ and $1/r^{10}$ attractive terms.

The experimental data are compared with the results of the semiclassical analysis in Fig. 3. The reduced cross sections, $Q_r=Q_e(\bar{g})/(Q_{\rm ref}X^{0.4})$ are plotted versus the inverse relative velocity for both the experimental data and the cross sections obtained from Eq. (8) using the best-fit parameters in Table I. While the fit as presented in Fig. 3(a) appears satisfactory, it can be seen in Fig. 3(b) that the experimental error (which is amplified by this type of plot) does not allow resolution of the glory extrema beyond $N=1$.

A second least-squares fit was performed with C_2 restricted to 0.4, which corresponds to pure $-C6/r^6$ long-range attractive potential. The fit was not satisfactory, but the parameters are also given in Table I. $C_2=0.4$ allows the use of Bernstein's method of analysis [18] to obtain the potential minimum, $-\varepsilon$, and its location, r_m. These results are also shown in Table I. The better fit with a smaller C_2 may be interpreted to mean that there are substantial contributions from $C8/r^8$ and $C10/r^{10}$ attractive-potential terms.

The results of Kerstel *et al.* [4] are also presented in Table I. There is substantial disagreement with the present results traceable primarily to a difference in the magnitude of the measured cross sections.

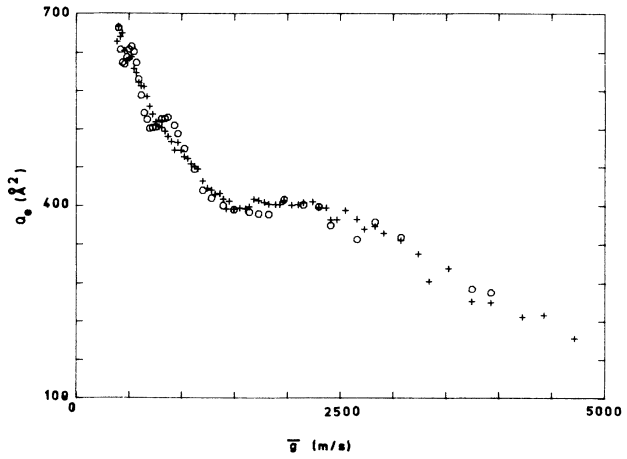

FIG. 4. Comparison of present data (+) with full quantum calculation of the cross section (○).

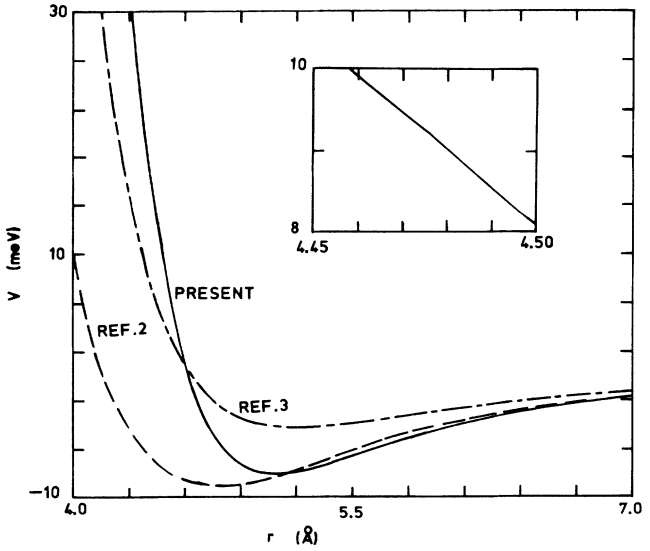

FIG. 5. Potential-energy functions. The parameters of the potential are given in Table II.

TABLE III. Summary of comparison with other results.

	This work						
	Semiclassical	Quantum	Ref. [2]	Ref. [3]	Ref. [4]	Ref. [21][a]	Ref. [22][a]
Γm (Å)	5.02	5.12	5.1	5.2	5.34	5.24	4.84
ε (meV)	6.74	8.22	9.1	4.2	8.28	8.86	9.05
$C6$ (a.u.)	370	274	449	280	480	540	390

[a]For K+Kr.

B. Quantum analysis

The data was also analyzed using a full quantum calculation of the phase shifts. This is a laborious calculation as the large reduced mass of the system and the relatively high velocity of the projectile require angular momenta as large as $1300\hbar$ to be used. The phase shifts were calculated by the integration of the Schrödinger equation using the Numerouv algorithm [19,20]. The integration started well inside the repulsive core of the potential and continued until the phase shifts converged to within 0.1% of a constant value.

Several trial potentials were used to find the potential that best represents the data. Except for the double Lennard-Jones potential [2],

$$V(r)=\begin{cases}\dfrac{AE}{B-A}\left[\left[\dfrac{R}{r}\right]^{B}\dfrac{-B}{A}\left[\dfrac{R}{r}\right]^{A}\right], & r<R\ ,\\ \dfrac{CE}{D-C}\left[\left[\dfrac{R}{r}\right]^{D}-\dfrac{7}{3}\left[\dfrac{R}{r}\right]^{C}\right], & r>R\ ,\end{cases} \tag{9}$$

all of the trial potentials were of the form

$$V(r)=HC(r)-C6/r^{6}-C8r^{8}-C10/r^{10}\ , \tag{10a}$$

where the following forms of the hard-core function $HC(r)$ were considered:

$$HC(r)=A/r^{B}\ , \tag{10b}$$

$$HC(r)=A\left[1-\frac{B}{r^{4}+C}\right]\exp(-Dr)\ , \tag{10c}$$

$$HC(r)=\begin{cases}(A/r)^{C}\ , & r<B\\ (B/r)^{D}(A/b)^{C}, & r>B\ .\end{cases} \tag{10d}$$

The potential given by Eqs. (10a)–(10d) provides a discontinuous slope or "kink" in the repulsive core at $r=B$. It was suggested by Martin *et al.* [1] that a peak they observed in their differential-cross-section measurement at a laboratory angle of 31° could be due to such a potential.

The constants in Eqs. (9) and (10) represented by capital letters were determined by the nonlinear least-squares procedure. The data were best represented by the potential (10a)–(10d). The quantum cross sections computed for this potential are compared with the experimental data in Fig. 4 using the parameters given in Table II. The potential (10a)–(10d) is compared with other experimentally determined potentials in Fig. 5. While the well depth of the present result agrees well with Winicur *et al.* [2], its position is in better agreement with Nenner [3]. The "kink" in the repulsive barrier at 4.48 Å is too slight to be easily discernible (see inset in Fig. 5). Cross sections calculated from potential (10a)–(10d) using the present

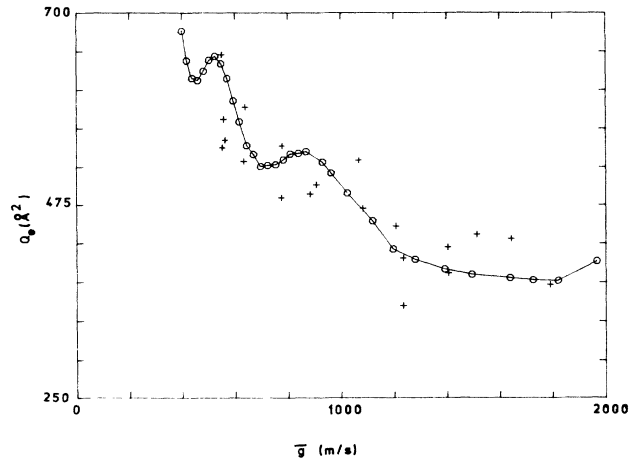

FIG. 6. Comparison of the cross sections from the full quantum fit of the present data (○) to the data of Nenner [3]. The line is drawn through the points of the full quantum fit to guide the eye. This figure illustrates the excellent agreement of our data and the data of Ref. [3].

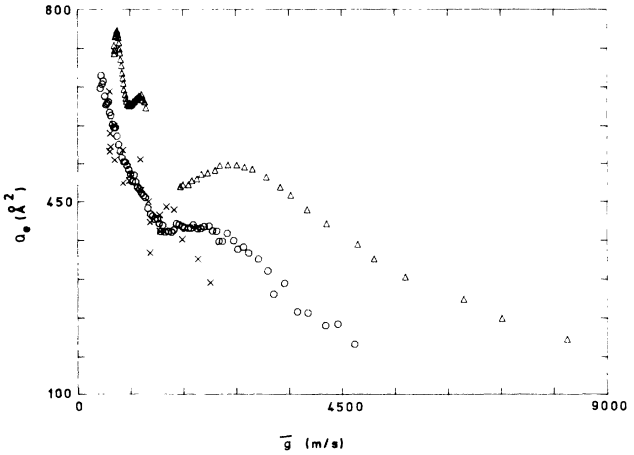

FIG. 7. The three measurements of the total elastic-scattering cross-section for the $Ar^{*}+Kr$ system. The data from Refs. [3] (×) and [4] (Δ) were digitized from enlargements of the data presented in those papers. The present data are shown as (○). See the text for a complete discussion.

best-fit parameters given in Table II are compared with the data of Nenner [3] in Fig. 6.

Table III gives a comparison of our ε, r_m, and $C6$ results from both semiclassical and full quantum analyses with other measurements. It can be seen there is little agreement between the various experiments. The present single-beam experiment is most accurate for determining the long-range attractive portion of the potential and the present value of $C6$ compares well with that of Nenner [3], who used a similar apparatus.

Figure 7 shows a comparison of the three measurements for the total elastic-scattering cross section for the Ar* + Kr system. The data of Nenner [3] and the data of Kerstel *et al.* [4] were digitized from enlargements of the figures presented in those papers. Krestel *et al.*'s [4] data was presented as relative inverse velocity versus relative cross section and this was deconvoluted to obtain the relative velocity versus absolute cross-section data as presented in Fig. 7. This figure shows that the most precise data available is the data of Krestel *et al.*[4]. It can be seen in Fig. 7 that our experimental data and the earlier data of Nenner [3] agree well. Nenner's [3] data exhibit larger statistical errors than our data, but essentially overlap our data. The shape of our measured cross sections and the position of the $n = 1$ glory oscillation is in satisfactory agreement with the more highly resolved measurement of Krestel *et al.* [4]. Krestel *et al.* [4] claim an absolute accuracy of 2.5% for their experiment. The excellent agreement between the present data and Nenner's [3] data would suggest that the absolute magnitude of the measurement of Krestel *et al.* [4] is in error. In a crossed-beam experiment, the value of the cross section depends on an accurate determination of the number density × length product for the target beam. An error in this determination would account for the observed difference in the measurements.

V. CONCLUSIONS

A potential-energy function [Eqs. (10a)–(10d)] has been obtained which represents the results of the present velocity-dependent total elastic-scattering-cross-section measurements. The van der Waals constant, $C6$, is in excellent agreement with the measurement of Nenner [3], but is much smaller than the electronically similar K + Kr ground-state system. While the long-range r^{-8} and r^{-10} terms proved especially important in obtaining a good fit to the experimental data, the discontinuity provided in the slope of the hard core was essentially removed by the fitting program, a smooth repulsive barrier giving a better fit.

*Present address: 5012 68th Street, Woodside, NY 11377.
†Present address: Physics Department, Florida State University, Tallahassee, FL 32306.

[1] D. W. Martin, T. Fukuyama, R. W. Gregor, R. M. Jordan, and P. E. Siska, J. Chem. Phys. **65**, 3720 (1976).
[2] D. H. Winicur, J. L. Fraites, and J. Bentley, J. Chem. Phys. **64**, 1724 (1976).
[3] T. Nenner, Entropie **42**, 142 (1971).
[4] E. R. T. Kerstel, C. P. J. W. Van Kruysdijk, J. C. Vlugter, and H. C. W. Beijerinck, Chem. Phys. **121**, 211 (1988).
[5] K. A. Hardy and J. W. Sheldon, Rev. Sci. Instrum. **52**, 1802 (1981).
[6] J. W. Sheldon and K. A. Hardy, Phys. Lett. **98A**, 332 (1983).
[7] K. A. Hardy and J.W. Sheldon, Phys. Rev. A **30**, 2761 (1984).
[8] M. E. Gersh, G. D. Sides, S. Y. Tang, and E. E. Muschlitz, Jr., J. Appl. Phys. **44**, 5356 (1973).
[9] G. Loriot and T. Moran, Rev. Sci. Instrum. **46**, 140 (1975).
[10] P. Kusch, J. Chem. Phys. **40**, 1 (1964).
[11] K. A. Hardy, E. Gillman, and J. W. Sheldon, J. Appl. Phys. **67**, 7240 (1990).
[12] R. N. Nelson and S. O. Colgate, Phys. Rev. A **8**, 3045 (1973).
[13] N. C. Lang, H. V. Lilenfield, and J. L. Kinsey, J. Chem. Phys. **55**, 3114 (1971).
[14] M. Bourne and J. LeCalve, J. Chem. Phys. **58**, 1452 (1973).
[15] L. G. Piper, J. E. Velazco, and D. W. Setser, J. Chem. Phys. **59**, 3323 (1973).
[16] B. C. Eu and W. S. Liu, J. Chem. Phys. **63**, 592 (1975).
[17] F. Von Busch, Z. Phys. **208**, 390 (1968).
[18] L. E. Landau and E. M. Lifshitz, *Quantum Mechanics* (Pergamon, London, 1959), p. 416.
[19] R. B. Bernstein, in *Molecular Beams,* edited by J. Ross (Wiley, New York, 1966).
[20] R. J. Munn, E. A. Maison, and F. J. Smith, J. Chem. Phys. **41**, 3978 (1964).
[21] U. Buck and H. Pauly, Z. Phys. **208**, 390 (1968).
[22] R. Duren, G. P. Rabbe, and C. Schlier, Z. Phys. **410**, 214 (1968).